

# Dual-detector X-ray fluorescence imaging of ancient artifacts with surface relief

Detlef-M. Smilgies,<sup>a\*</sup> Judson A. Powers,<sup>b</sup> Donald H. Bilderback<sup>a,c</sup> and Robert E. Thorne<sup>b</sup>

<sup>a</sup>Cornell High Energy Synchrotron Source (CHESS), Cornell University, Ithaca, NY 14853, USA,

<sup>b</sup>Physics Department, Cornell University, Ithaca, NY 14853, USA, and <sup>c</sup>School of Applied and Engineering Physics, Cornell University, Ithaca, NY 14853, USA. E-mail: dms79@cornell.edu

Interpretation of X-ray fluorescence images of archeological artifacts is complicated by the presence of surface relief and roughness. Using two symmetrically arranged fluorescence detectors in a back-reflection geometry, the proper X-ray fluorescence yield can be distinguished from intensity variations caused by surface topography. This technique has been applied to the study of Roman inscriptions on marble.

© 2012 International Union of Crystallography  
 Printed in Singapore – all rights reserved

**Keywords:** fluorescence imaging; inscriptions; archeology.

## 1. Introduction

X-ray fluorescence (XRF) imaging is emerging as a powerful technique for extracting information from archeological inscriptions (Harbottle *et al.*, 1986; Janssens *et al.*, 2000; Powers *et al.*, 2005, 2009) and other artifacts. For Roman inscriptions on marble, trace-element maps facilitated the detection of iron (Fe) atoms from the original chisel work and residues of pigments originally used to paint letters and background. On weathered stones, a lead-oxide-based red pigment commonly used in lettering is often no longer visible. But the lead XRF signal can often be easily detected, even in cases where the stone is weathered and worn below its original inscribed surface, potentially allowing recovery of text (Powers *et al.*, 2005; Powers, 2007).

However, inscriptions and other archaeological artifacts generally do not have smooth flat surfaces, either by original design (*e.g.* chiseled letters or the curved surfaces of pottery) or as a result of weathering and other kinds of damage. This surface topography can corrupt the interpretation of XRF measurements of elemental distributions. Fig. 1(a) shows detail from a Roman inscription (Volcelia) from the collections of the Frances Lehman Loeb Art Center at Vassar College. Pronounced optical ‘shadowing’ is clearly seen near deeply inscribed lines. Variations in local surface orientation cause differences in XRF intensity obtained from smooth and rough surfaces. Fluorescence measured from one point on a surface can also be attenuated if it must propagate through an adjacent raised portion on its way to the detector. These topography-related intensity variations can swamp variations owing to elemental concentration and make small enhancements of trace-element concentrations near surfaces, which may be the only remnant of important information, difficult to discern. Here we show how a dual-detector scheme can be used to differentiate between concentration- and topography-related fluorescence intensity variations.

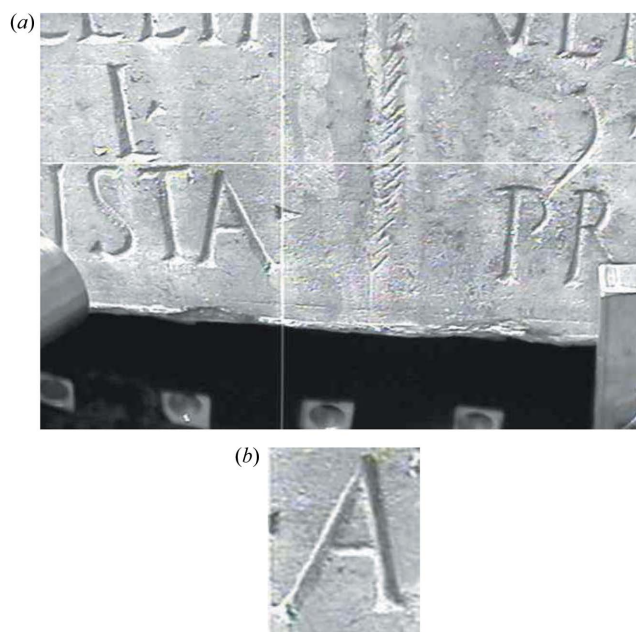


**Figure 1**

(a) Still image from a video camera showing the Volcelia stone mounted with clamps on a padded easel. Rubber padding, both on clamps and easel, protected the artifact. The cross-hair of the video camera was trained on the optical fluorescence (not shown) of the marble substrate where the beam hit the sample. (b) A detailed view of the letter ‘A’ used for this study.

## 2. Method

A common set-up for synchrotron-based XRF imaging orients the surface under examination at 45° to the incident beam and the detector at 90° in the horizontal plane. Since synchrotron radiation is horizontally polarized, this configuration suppresses Compton and Rayleigh scattering (Gordon, 1982; Gordon & Jones, 1985), an important consideration when using count-rate-limited detectors such as Si(Li) and Ge

detectors. However, the introduction of high-performance Si drift detectors, such as the XFlash detector (Roentec) used in this study, has eased this restriction.

In our experiments on large and heavy stones (about 1 m × 0.5 m and 50 kg weight for the largest sample) with deeply chiseled features, we chose instead to work in a quasi-back-scattering geometry, with the sample oriented normal to the incident beam and the X-ray detector at about 135° relative to the incident beam (Powers *et al.*, 2005). The larger scattering angle further reduced Rayleigh and Compton scattering. Moreover, the shading of XRF signals in the deep part of the inscriptions is mostly avoided. Detector saturation, owing to the high calcium (Ca) XRF background generated by the marble substrate, was resolved by using a high-count-rate high-resolution XRF detector.

According to Lambert’s law (Lambert, 1760; Worthing, 1912; Aslan *et al.*, 2007) the intensity of radiation emitted from a finite area on a flat surface varies with observation angle as

$$I(\theta) = I_0 \cos(\theta), \tag{1}$$

where  $\theta$  is the angle between the detector and the surface normal. For a rough surface or a surface with relief we define  $\theta$  as the angle between the detector and the *local* surface normal and  $\theta_0$  as the angle between the detector and the normal to the *average* surface. If we add a second detector at the mirror-symmetric  $-\theta_0$  position (see Fig. 2), a deviation  $\delta$  of the local surface  $\theta$  from the average surface  $\theta_0$  as viewed by the first detector corresponds to a deviation  $-\delta$  at the second detector. Considering a Taylor expansion of the cosine function with regard to a small deviation  $\delta$  from the detector angle  $\theta_0$ ,

$$\cos(\theta_0 + \delta) = \cos(\theta_0) + \sin(\theta_0) \delta, \tag{2}$$

we have the following signal combinations,

$$\begin{aligned} [I_1(\theta) + I_2(\theta)]/I_0 &= 2 \cos(\theta_0), \\ [I_1(\theta) - I_2(\theta)]/I_0 &= 2 \sin(\theta_0) \delta. \end{aligned} \tag{3}$$

Thus, the proper XRF yield  $Y = I_1 + I_2$  can be separated from surface relief effects  $R = I_1 - I_2$  in a simple way (and without knowledge of the local deviation angle  $\delta$ ), as long as the linear approximation holds. Even beyond the linear regime the dual

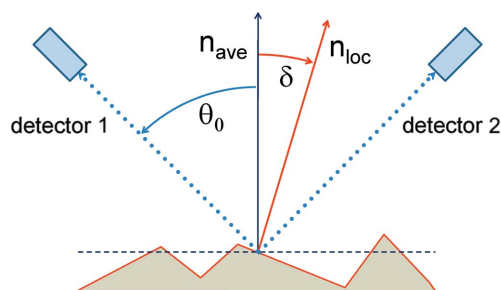


**Figure 2** Dual-detector scheme for measuring XRF emission from a rough surface.  $\theta_0$  is the angle between detectors 1 or 2 and the normal vector  $\mathbf{n}_{ave}$  of the average surface plane (dashed line). The blue dotted arrows denote the directions along which fluorescent radiation is detected. The local surface normal  $\mathbf{n}_{loc}$  deviates by an angle  $\delta$  from  $\mathbf{n}_{ave}$ , and the detectors measure fluorescence at angles  $\theta_0 \pm \delta$  from the local surface normal.

detector set-up remains useful in highlighting the relief effect qualitatively, even though perfect relief compensation cannot be achieved without knowing the local  $\delta$  and surface height  $h$  throughout the examined area. If the dual single-element detectors are replaced by symmetric linear detector arrays, even higher-quality quantitative information can be obtained. Note that  $Y$  and  $R$  are not sensitive to any component of the local tilt  $\delta$  that is perpendicular to the plane defined by the average surface normal and the detector direction. A second detector pair rotated 90° about the incident beam direction relative to the first pair can be added to quantify and correct for this tilt component.

The above argument assumes that the trace elements generating the fluorescence signals of interest are located right at the surface. When the sample is encrusted or covered with patina, absorption of fluorescence signals by this layer needs to be taken into account. As discussed by Gordon (1982) and Fiorini *et al.* (2002) for a flat surface, the result is a modified angular dependence of the XRF signal. Note that the dual detector method is robust with regard to such modification as long as the angular dependence remains reasonably smooth and monotonic, so that the Taylor expansion still results in a reasonable linearization within the angle range of the surface relief.

### 3. Application

Experiments were performed at the Cornell High Energy Synchrotron Source (CHESS), on station D1. Using a multi-layer monochromator, the station delivered  $10^{11}$  photons  $s^{-1}$  at an X-ray energy of 17 keV into a 1 mm × 1 mm beam. The incident-beam intensity was monitored with an ion chamber for normalization. XRF signals were detected with two Si drift detectors (Roentec X-Flash). These detectors had a spectral resolution of 180 eV up to a maximum count rate of  $10^5$  counts  $s^{-1}$ . The high count rate and good energy resolution were essential in order to detect small trace-element signals hidden among the intense calcium XRF from the marble substrate which for the most part consists of calcite ( $CaCO_3$ ).

The sample to be examined was mounted on an  $x$ - $z$  scanning stage attached to a sturdy table. The heavy sample was supported by a rubber-padded base plate and held to a rubber-padded aluminium backing plate with a 1" × 1" pattern of threaded holes using rubber-padded clamps arranged according to the size and shape of the sample. Marble shows optical fluorescence when hit by an intense X-ray beam. A video camera monitored the sample and this fluorescent spot during scanning (Fig. 1), and an electronic cross-hair was aligned with the spot. This allowed easy positioning of an area of interest with respect to the X-ray beam, and approximate registration of optical and XRF images.

The XRF detectors were mounted on  $x$ - $z$  stages clamped to the incident beam optical table. The detector angles relative to the average sample surface plane were determined using a protractor and the angles relative to the incident beam set to 135°. The 3.2 mm-diameter, 10 mm<sup>2</sup> active area of each

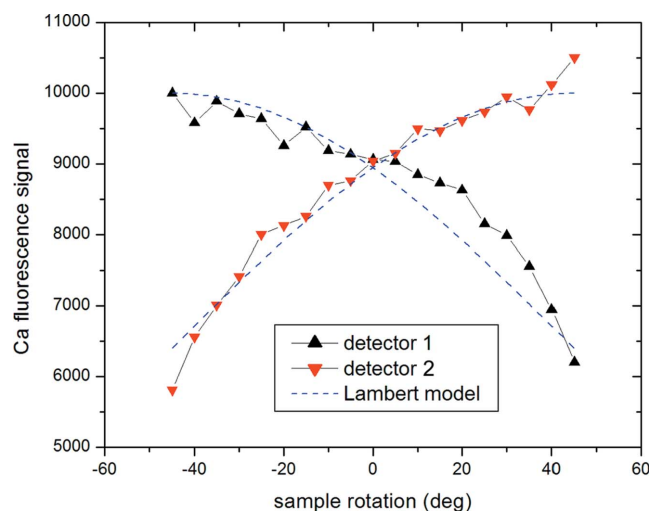


**Figure 3** Calibration of the dual-detector set-up using a flat marble substrate on a rotation stage. The relative rotation angle of 0 corresponds to normal incidence on the substrate. The XRF yield of the Ca  $K_{\alpha}$  line measured at the two detectors was fitted to the Lambert model described in the text.

detector was placed 360 mm from the sample, resulting in an angular acceptance/resolution of 8 mrad. A 310 mm-long snout with a Be window between detector and sample left a 50 mm working distance between snout tip and sample. The symmetry of the relative detector alignment was tested using a flat smooth piece of marble mounted on a rotation stage. The signal measured by each detector was maximized using each detector's  $x$  and  $z$  translations. Ca  $K_{\alpha}$  fluorescence was then measured as a function of rotation angle (Fig. 3). This calibration gave a relative scale factor for the two detectors, which accounted for differences in detector sensitivity, in sample-detector distance and in detector alignment. With the given X-ray illumination and detection conditions, the escape depth of the Ca  $K_{\alpha}$  signal (3.7 keV) was about 20  $\mu\text{m}$  assuming a pure calcite matrix, the main component of marble. XRF from iron traces (6.4 keV) in this matrix has about the same escape depth owing to increased absorption above the Ca  $K$ -edge at 4.0 keV (CXRO, 2012).

With the sample mounted, XRF spectra were collected at each point of a grid scan whose step size was set equal to the 1 mm  $\times$  1 mm beam size. An in-house macro written for the *SPEC* control software (Swislow, 1985) acquired spectra for each detector simultaneously and wrote these spectra to separate files. Spectra were normalized using an ion chamber as an incident-beam monitor. Each X-ray fluorescence line of these spectra was fitted, and the integrated intensity of Ca  $K_{\alpha}$  and Fe  $K_{\alpha}$  fluorescent lines was determined and plotted using a false-color scale using a *MatLab* program developed by Rong Huang. Two processed images were obtained from the dual detector set-up. The XRF intensities were added to obtain the relief-corrected yield image  $Y$ , or subtracted to obtain the relief signal image  $R$ .

Fig. 1 shows the Roman epigraph Volcelia examined in this study. The epigraph has guide rules as well as a series of small decorative marks. The chiseled text has a sharp 'V' profile, about 3 mm deep; the decorative marks are less than 1 mm

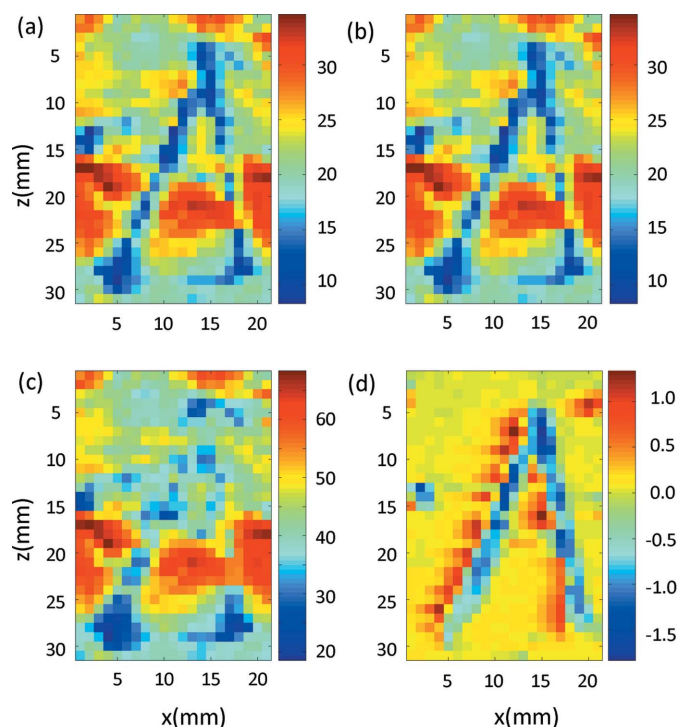


**Figure 4** Calcium XRF from Volcelia: raw signal from (a) detector 1 and (b) detector 2, (c) sum signal and (d) difference signal. The compensated Ca sum image mostly shows fluctuations in Ca content close to the surface, while the relief effect, highlighted in the difference image, is mostly removed. One pixel corresponds to the beam size of 1 mm  $\times$  1 mm.

deep. Fig. 4 shows four images of Ca XRF obtained with the dual-detector set-up: the two single-detector images (top), as well as sum  $Y$  and difference  $R$  images (bottom). Under the ideal conditions assumed in our approximation, we expect  $Y$  to be essentially homogeneous, and all relief features to appear in  $R$ . In fact, we find that surface relief effects are mostly absent from the compensated sum image. The residual Ca fluorescence fluctuations may arise from fluctuations in the Ca content near the surface owing to, for example, weathering or cleaning, from absorption by a surface layer (*e.g.* associated with tool wear, residual paint or encrustation, especially in the deeply inscribed serifs), and possibly also from direct shadowing or blocking of emitted fluorescence by adjacent elevated regions (*e.g.* in the deeply inscribed serifs). Note that the horizontal stroke connecting the two legs of the 'A' is largely invisible in all four XRF images. The stroke runs almost parallel to the plane formed by the incident beam and detectors, and the local inclination angles  $\delta$  of its surface are almost perpendicular to this plane. This relief could be detected by adding a second pair of detectors oriented perpendicular to the first set.

Fig. 5 shows corresponding Fe XRF images. The Fe difference image  $R$  shows some effect of relief. But, unlike with Ca, the Fe sum image  $Y$  shows a strong correlation with the difference image. This indicates that (unlike for Ca) the Fe concentration in the surface is indeed correlated with inscribed regions, and so is likely due to tool wear or painting. The horizontal stroke connecting the two legs of the 'A' is

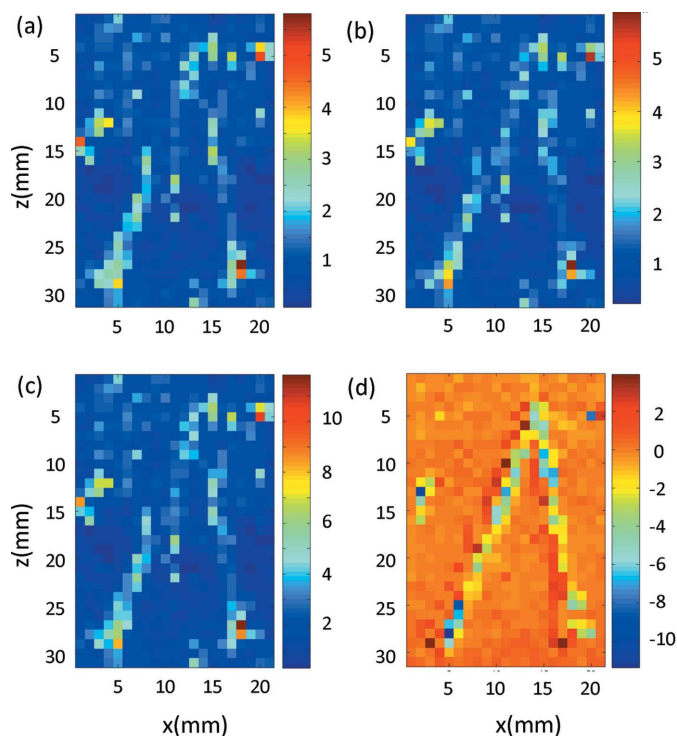


**Figure 5** Iron XRF from Volcelia: (a) detector 1, (b) detector 2, (c) sum and (d) difference. Unlike the Ca sum image the compensated Fe sum image closely follows the surface relief signal of the difference image. This further supports the correlation of Fe with chisel marks and inscription. The pixel size equals the beam size of 1 mm × 1 mm.

largely absent, except for one spot to the left of the letter’s center, in the Fe sum images. As can be seen in Fig. 1(b), the horizontal stroke is less deeply incised than the rest of the letter, and so there may be fewer tool residues; it is also more accessible to erosion and other processes that remove surface layers. In our XRF measurements on more than 20 marble inscriptions, tool and paint residues are generally most pronounced in the most deeply incised regions.

These results demonstrate that the separation of proper XRF yield  $Y$  from surface relief  $R$  facilitated by the dual-detector method can assist in interpreting XRF images from rough surfaces or surfaces with substantial relief. This enhances the utility of XRF imaging as an analytical tool for trace-element analysis, in particular for surfaces that are not flat, as encountered in archeology and art history samples, but also in environmental science. Recently, De Samber *et al.* (2010) introduced a dual-detector scheme for compensating self-absorption in XRF imaging of a small three-dimensional object. Dual- and multiple-detector schemes should thus help

overcome well known limitations of single-detector XRF methods.

We would like to thank Kevin Clinton and Nora Dimitrova of the Cornell Classics Department who have provided a wealth of information about the ancient world and epigraphy. We thank the Frances Lehman Loeb Art Center at Vassar College for providing the Volcelia stone. We are indebted to Rong Huang (CHESS) for the use of his XRF analysis program. We thank Arthur Woll (CHESS) for use of his large scanner and commenting on the manuscript. We thank the reviewers for their suggestions. This work has been supported by the Office of the Vice Provost for Research, by the National Science Foundation (DMR 08-05240) and by the Kress Foundation. This work is based upon research conducted at the Cornell High Energy Synchrotron Source (CHESS) which is supported by the National Science Foundation, the National Institute of Health and the National Institute of General Medical Sciences under award DMR- 0936384.

**References**

Aslan, K., Malyn, S. N. & Geddes, C. D. (2007). *Analyst*, **132**, 1112–1121.

CXRO (2012). Center for X-ray Optics at Lawrence Berkeley Laboratory, *X-ray attenuation length*, [http://henke.lbl.gov/optical\\_constants/atten2.html](http://henke.lbl.gov/optical_constants/atten2.html).

De Samber, B., Vanblaere, S., Evens, R., De Schamphelaere, K., Wellenreuther, G., Ridoutt, F., Silversmit, G., Schoonjans, T., Vekemans, B., Masschaele, B., Van Hoorebeke, L., Rickers, K., Falkenberg, G., Szaloki, I., Janssen, C. & Vincze, L. (2010). *Powder Diffr.* **25**, 169–174.

Fiorini, C., Gianoncelli, A., Longoni, A. & Zaraga, F. (2002). *X-ray Spectrom.* **31**, 92–99.

Gordon, B. M. (1982). *Nucl. Instrum. Methods*, **204**, 223–229.

Gordon, B. M. & Jones, K. W. (1985). *Nucl. Instrum. Methods Phys. Res. B*, **10–11**, 293–298.

Harbottle, G., Gordon, B. M. & Jones, K. W. (1986). *Nucl. Instrum. Methods Phys. Res. B*, **14**, 116–122.

Janssens, K., Vittiglio, G., Deraedt, I., Aerts, A., Vekemans, B., Vincze, L., Wei, F., Deryck, I., Schalm, O., Adams, F., Rindby, A., Knöchel, A., Simionovici, A. & Snigirev, A. (2000). *X-ray Spectrom.* **29**, 73–91.

Lambert, J. H. (1760). *Photometria sive de mensura et gradibus luminis, colorum et umbrae*. Augustae Vindelicorum, V. E. Klett, Augsburg.

Powers, J. (2007). Masters thesis, Cornell University, USA.

Powers, J., Dimitrova, N., Huang, R., Smilgies, D.-M., Bilderback, D., Clinton, K. & Thorne, R. E. (2005). *Z. Papyrol. Epigr.* **152**, 221–227.

Powers, J., Smilgies, D.-M., Geil, E. C., Clinton, K., Dimitrova, N., Peachin, M. & Thorne, R. E. (2009). *J. Archeol. Sci.* **36**, 343–350.

Swislow, G. (1985). *Certified Scientific Software*, <http://www.certif.com/>.

Worthing, A. G. (1912). *Astrophys. J.* **36**, 345–361.